International Journal of Nanomedicine

Dovepress

open access to scientific and medical research

Open Access Full Text Article

ORIGINAL RESEARCH

A Pegylated Liposome Loaded with Raddeanin A for Prostate Cancer Therapy

Kang He[1,*], Taiwei Wang[1,*], Junyu Chen[2,*], Xuemiao Huang[1], Zeyu Wang[1], Zhaoyun Yang[1], Kai Wang[1], Weixin Zhao[2], Jian Jiang[1], Lijing Zhao[1]

[1]Department of Rehabilitation, School of Nursing, Jilin University, Changchun, Jilin, 130021, People's Republic of China; [2]Department of Gynaecology and Obstetrics, The Second Hospital, Jilin University, Changchun, Jilin, 130041, People's Republic of China

*These authors contributed equally to this work

Correspondence: Lijing Zhao; Jian Jiang, School of Nursing, Jilin University, 965 Xinjiang Street, Changchun, Jilin, 130021, People's Republic of China, Email zhao_lj@jlu.edu.cn; jiangjian91@jlu.edu.cn

Introduction: Raddeanin A (RA), a potent triterpenoid extracted from Anemone raddeana Regel, has a moderate therapeutic effect on prostate cancer (PCa), correlating with serious biological toxicity. Therefore, a RA-loaded PEGylated liposome drug delivery system was devised in this study.

Methods: Hydrogenated soybean phospholipids (HSPC), 1,2-distearoyl-sn-glycero-3-phosphoethanolamine-N-Polyethyleneglycol-2000 (sodium salt) (DSPE-PEG2k), cholesterol (CHO), and RA were utilised to prepare a RA-loaded liposome (LRA) drug delivery system via the thin film hydration technique., The drug loading content was confirmed by high performance liquid chromatography. Dynamic light scattering was employed to evaluate the drug's particle size and stability. Methyl tetrazolium, colony formation, and Western blot (WB) were used in vitro to elucidate the inhibitory effect and mechanism of LRA on prostate cancer cells. Finally, xenograft model was used to confirm the tumor-inhibiting efficacy, clarify the mechanism, and determine the biosafety in mice.

Results: LRA has stable physicochemical properties and a diameter of 173.5 15.3 nm. LRA inhibited the growth of prostate cancer cells in a dose- and time-dependent manner. LRA can substantially reduce the expression of AR and HMGB1, induce apoptosis, regulate the expression of cell cycle-related proteins in vitro and in vivo. The results of the biosafety tests demonstrated that LRA effectively reduced the adverse effects of RA.

Conclusion: As a drug delivery system, LRA could effectively and safely inhibit the progression of prostate cancer.

Keywords: prostate cancer, liposome, Raddeanin A, HMGB1, AR

Introduction

Prostate cancer (PCa) is one of the most common cancers in men, with more than 260,000 new cases and 34,500 deaths estimated in the USA in 2022.[1,2] Androgen receptors (AR) play a decisive role in the progression of PCa. Androgen deprivation therapy (ADT) aims to inhibit the development of prostate cancer by antagonizing androgen production, and binding to AR remains the mainstay of treatment for PCa.[3] However, most PCa patients develop potential castration-resistant prostate cancer (CRPC) after 18–36 months of ADT, and CRPC is an important cause of drug resistance and death in patients.[4] Multiple molecular mechanisms may be involved in the progression of CRPC, but current findings suggest that AR play an important role in this process[5,6] in which the androgen produced by the tumor is considered a critical factor for the continuous activation of the AR in CRPC.

High-mobility Group Protein B1 (HMGB1) is an important mediator of the activation of transcription factor signaling pathways. It can regulate gene transcription by promoting the binding of transcription factors and specific DNA sequences, and participates in the occurrence and development of various tumors.[7] Our previous study found that the expression of HMGB1 was significantly increased in PCa specimens, which may be strongly correlated with AR expression. In addition, HMGB1 can reactivate AR signaling and directly interact with AR to promote CRPC

Received: 26 May 2023
Accepted: 17 July 2023
Published: 21 July 2023

Graphical Abstract

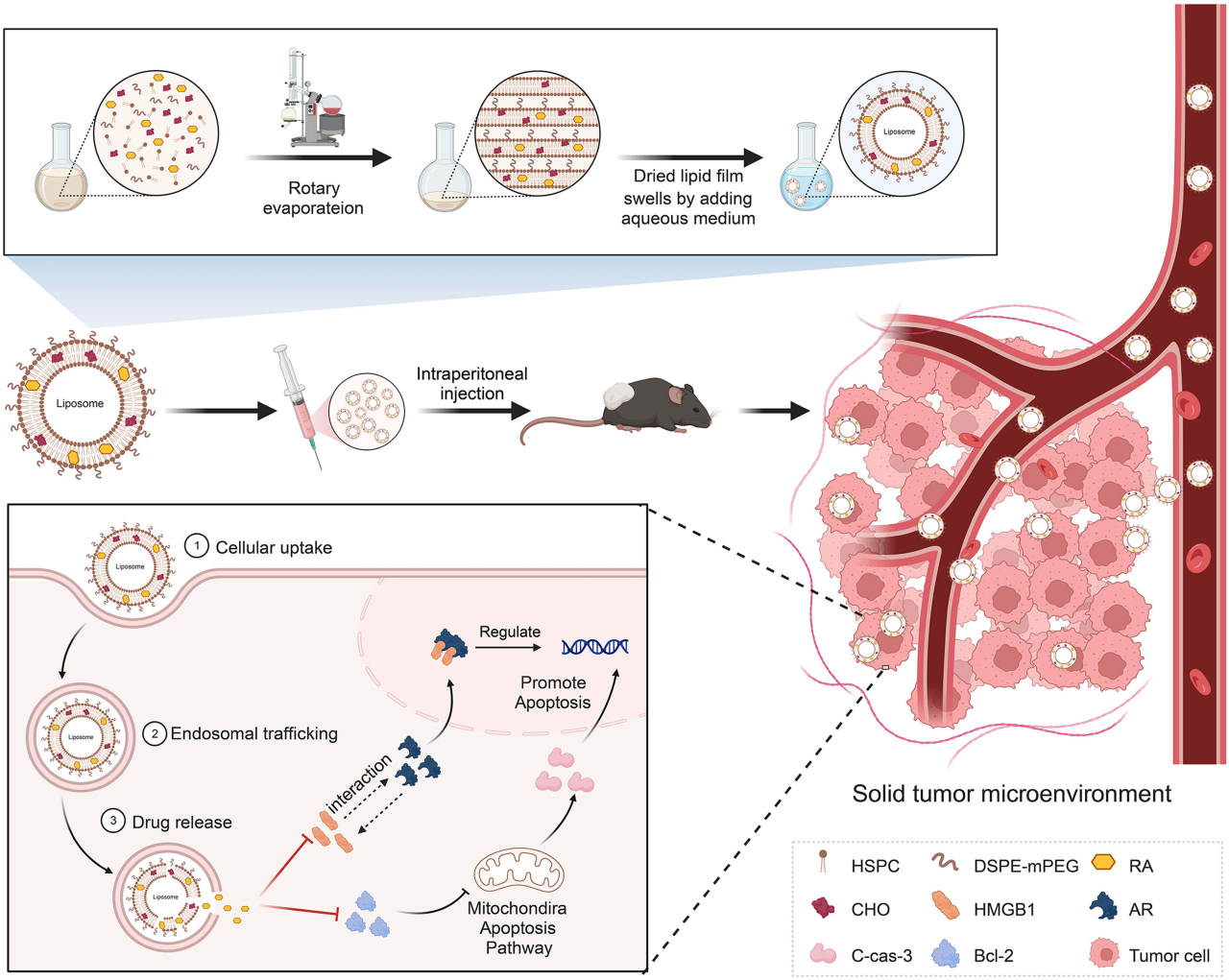

development in a non-androgenic manner.[8] A surge of research has shown that during ADT treatment, AR are reactivated in numerous ways in vivo, such as by AR gene mutation, to ensure that AR could still play an important role in the environment of persistently low androgen levels.[2] Therefore, there is an urgent need to develop more effective therapeutic agents.

Raddeanin A (RA), a natural triterpenoid extracted from *Anemone raddeana Regel*, has significant antitumor effects on various tumors.[9–12] In our previous study, RA was shown to target both full-length AR (AR-F) and splice variants of AR (AR-V), and inhibit the growth of 22Rv1 human prostate cancer cells in vitro. Moreover, RA-induced inhibition of CRPC cells appeared to be AR-dependent but not androgen-dependent.[13] Pharmacokinetic investigations have shown that the plasma concentration of RA is lower after oral administration than after intravenous or intraperitoneal administration.[14,15] However, preliminary experiments have also shown that after intraperitoneal injection of RA, mice exhibit significant biological toxicity, such as loss of body weight and abnormal body posture. Thus, it is necessary to determine the optimal route for RA administration and delivery system.

Liposomes, initially reported in 1964,[16] are bilayer vesicles composed of multiple amphiphilic lipid molecules. The particular hollow ring structure, owing to the presence of hydrophilic and hydrophobic regions, offers a strong backing force for liposomes as drug carriers.[17] To date, liposomes have been extensively explored in many research studies as drug

delivery vehicles due to manifest properties such as biocompatibility,[18] biodegradability,[19] low biotoxicity,[20] extending the retention time of the maximum plasma concentration of drug,[21] as well as targeting ability.[22] In previous studies, epigallocatechin-3-gallate (EGCG) coated with polyethylene glycol gelatin hyaluronic acid (HA) nanoparticles was used for targeted treatment of prostate cancer, which was proved to be effective in inhibiting the G2/M phase cycle arrest of prostate cancer cells and inhibiting cell growth. Moreover, liposome medications can specifically bind CD44 receptor and enhance the apoptotic activity of cancer cells.[23] In addition, anchoring a prostate-specific membrane antigen to a lipid nanoparticle system designed with a pegylated lipid has been shown to be effective in increasing the accumulation of drugs in prostate tumors and reducing the toxicity of drugs to other organs in rodents.[24] There is also a recent study using calcium alginate nanoparticles coated with curcumin and resveratrol for targeted treatment of prostate cancer. This liposome drug showed good stability, and it was proved that the cumulative release amount within 24 hours could reach 87.6%, which could be effectively taken up by tumor cells, and had potent tumor cytotoxicity.[25] Different functions of liposomes can be achieved using various synthesis strategies. The drug delivery capability of liposomes is affected by many factors including lipid composition, surface modification, particle size, and particle stability.[26]

In this study, hydrogenated soybean phospholipids (HSPC), 1.2-distearoyl-sn-glycero-3-phosphoethanolamine-N-Polyethyleneglycol-2000 (sodium salt) (DSPE-PEG_{2k}), cholesterol (CHO), and RA were used to prepare an RA-loaded liposome (LRA) drug delivery system using the thin film hydration method. The therapeutic effects and safety of LRA for PCa have been demonstrated both in vivo and in vitro.

Materials and Methods

Chemicals and Reagents

Raddeanin A (RA, purity≥98%), trehalose (purity≥98%), Rhodamine B (Rh, purity≥98%), HSPC (purity≥95%), and CHO (purity≥98%) were purchased from Yuanye Bio-Technology (Shanghai, China). DSPE-$mPEG_{2k}$ was purchased from Cayman Chemical Co. (Ann Arbor, MI, USA). The Annexin V-FITC/PI cell apoptosis detection kit and TUNEL Cell Apoptosis Detection Kit were purchased from TransGen Biotech (Beijing, China). The MTT reagent kit, hematoxylin-eosin (H&E) Staining Kit, and Masson's trichrome staining kit were purchased from Solarbio Science and Technology Company (Beijing, China). Antibodies against GAPDH (Cat# 10494-1-AP) and Bcl-2 (Cat# 26593-1-AP) were purchased from Proteintech (Wuhan, Hubei, China). Anti-cleaved-Caspase-3 antibody (Cat#AF7022), Ki67 (Cat#AF0198), and HRP-conjugated Goat Anti-Rabbit IgG secondary antibodies (Cat#S0001) were purchased from Affinity Bioscience (Changzhou, Jiangsu, China). Anti-HMGB1 (Cat#ab18256) and anti-AR (Cat#ab74272) antibodies were purchased from Abcam (Cambridge, MA, USA). The PSA Elisa Kit (Cat#MM-0469M1) was purchased from Jiangsu Meimian Industrial Co., Ltd. (Jiangsu, China).

Preparation of RA Liposome

HSPC, CHO, DSPE-PEG_{2k}, and RA were dissolved in methyl alcohol in a molar ratio of 3.3:2.3:0.3:1. The solvent was then removed using a rotary evaporator to obtain the lipid films. Liposomes were prepared by hydrating the dried lipid films with deionized water and stirring for 120 min, followed by ultrasonication (500 W) for 120 min. Free RA was removed by dialysis (dialysis bag, MWCO 3500 Da) after stirring for 12 h. The dialysis solution was filtrated through a 0.45 μm filter membrane and freeze-dried with 2% trehalose (w/v) to obtain RA liposome (LRA). The drug loading content (DLC%) was confirmed by high performance liquid chromatography (HPLC). The equation for DLC% was as follows: DLC% = (RA weight) / (Total RA liposome weight) × 100%. HPLC conditions were as follows: the mobile phase was acetonitrile and H_2O (containing 0.05% acetic acid) at a flow rate of 1 mL/min and the ratio of acetonitrile/H_2O was 65/35. An ultraviolet (UV) detector was used with absorption wavelength 256 nm to measure the quantity of RA.

The Release of LRA

A total of 3 mg freeze-dried LRA was dissolved in 3 mL phosphate buffered saline (PBS) at different pH (pH 7.4, pH 6.8), placed in dialysis bags (MWCO 3500 Da), and incubated with 27 mL released media at 37 °C with shaking at

100 rpm. At different time points (0, 1, 4, 24, 48, and 72 h), 3 mL of the incubated solution was removed and replaced with fresh medium. The released RA was analyzed using HPLC after freeze-drying.

The Stability of LRA

A sample of 1 mg freeze-dried LRA was dissolved in 1 mL pH 7.4 PBS buffer, and the solution was shaken at 100 rpm at 37 °C. The diameter of the LRA was measured by dynamic light scattering (DLS) at different time points (0, 1, 2, 6, and 24 h).

Cellular Endocytosis Assay

To investigate the cellular uptake of LRA, RA and Rhodamine B (Rh) co-loaded liposomes (LRA/Rh) were prepared. Rh was dissolved in methyl alcohol solution containing HSPC, CHO, DSPE-mPEG$_{2k}$, and RA. The Rh/RA molar ratio was 0.03:1. The preparation method for LRA/Rh was the same as that for LRA.

RM1 cells were cultured in 6-well plates at a density of 3×10^5 cells/well and treated with 1.5 μL or 3 μL of LRA/Rh for 0.5, 3, and 5 h. At each time point, the medium containing the Rh-labeled liposomes was removed, and the cells were washed twice with PBS. A fluorescence microscope (Olympus, Tokyo, Japan) was used to observe the localization of Rhodamine B.

Cell Culture

The mouse prostate cancer cell line RM1 and human prostate cancer cell line 22Rv1 were purchased from Procell Life Science & Technology Company (Wuhan, Hubei, China). The cells were cultured in RPMI 1640 medium (HyClone, USA) supplemented with 10% fetal bovine serum (FBS; Gibco, USA), 100 units/mL penicillin, and 100 μg/mL streptomycin in a humidified 5% CO_2 atmosphere at 37 °C.

Cell Viability Assay

The cytotoxicity of RA and LRA in RM1 and 22Rv1 cells was measured using an MTT assay. Briefly, cells were seeded in a 96-well plate at a density of 3×10^3 cells per well and incubated with RA or LRA for 24, 48, and 72 h. The medium was then replaced, and 5 mg/mL of methyl tetrazolium (MTT) was added to each well and incubated for another 4 h. Subsequently, DMSO was added to each well to dissolve the precipitate. The absorbance was quantified at 570 nm (Cytation 5; Biotek, Winooski, VT, USA).

Colony Formation

The cells were seeded in 6-well plates at a density of 600 cells/well. After being treated with different concentrations of RA or LRA for 2 weeks, the cells were fixed with 4% paraformaldehyde for 15 min at room temperature and stained with Wright-Giemsa stain working solution under the guidance of an instruction manual. Cell clusters with more than 50 cells were counted as a colony. Cell clonality was calculated as follows: number of colonies / number of plated cells.

Apoptosis Assay and Cell Cycle Assay

Cells were cultured in 6-well plates (3×10^5 cells/well), treated with RA or LRA for 24 and 48 h, and suspended in PBS. For the apoptosis assay, the cells were incubated in 100 μL Annexin V binding buffer containing 5 μL Annexin V-FITC and 5 μL PI for 15 min at room temperature in the dark. After adding 400 μL of binding buffer, the stained samples were analyzed using the BD FACS Calibur (BD, San Jose, CA, USA). For cell cycle assay, the cells were fixed with pre-chilled cell fixative solution (70% ethanol) for 1 h at −20°C, followed by suspension in staining solution (50 μg/mL propidium iodide, 100 μg/mL RNase-A, and 0.2% Triton X-100) for 30 min in the dark. The stained samples were analyzed using the BD FACS Calibur, and the results were visualized using Modfit LT 5 software.

Western Blot Analysis

The cultured cells and tumor tissues were collected and frozen at −80 °C, and total proteins were extracted using RIPA Lysis Buffer (Beyotime, Shanghai, China) and quantified with the Coomassie Plus (Bradford) Assay Kit (Thermo Scientific, Cat#23236). Western blot analysis was performed according to previous studies.[27] After separation through

a precast BIS-Tris Gel (4–20%, Cat#abs9384, Absin, Shanghai, China), proteins were transferred onto PVDF membranes. The membranes were blocked with 5% skimmed milk for 45 min at room temperature and then incubated waveringly with primary antibodies, including anti-HMGB1 (1:1000), anti-GAPDH (1:20,000), anti-Bcl-2 (1:2000), anti-cleaved-Caspase-3 antibody (1:1000), and anti-AR antibody (1:100) at 4 °C overnight. Subsequently, the membranes were incubated with HRP-conjugated secondary antibodies (1:10,000) at room temperature for 1 h. Finally, the bands were visualized by the ECL method using a ChemiScope 6000 imaging system (Clinx Science Instruments, China) and quantified using ImageJ software. The assay was independently repeated three times.

Animal Study

The in vivo experiments were conducted using protocols and conditions approved by the Experimental Animal Ethics Committee of Jilin University (Changchun, China). Animal experiments were complied with the arrival guidelines and the National Institutes of Health Guidelines for the Care and Use of Laboratory Animals. Male C57BL/6 mice were purchased from Beijing Unilever Laboratory Animal Co., LTD and reared in a group of five animals per cage at a temperature of 22 ± 1 °C and a 12 h light/dark cycle with access to food and water ad libitum.

To prepare the RM1 xenograft model, 2×10^6 RM1 cells were injected subcutaneously into the right back of 6-week-old male C57BL/6 mice. When the tumor volume reached 100–150 mm^3, the mice were randomly divided into three groups – control, RA, and LRA – with five mice in each group, and intraperitoneally injected with 200 μL saline, RA (4 mg/kg), or LRA (4 mg/kg, on an RA basis) once every three days respectively. RA and LRA were both dissolved in saline solution.

The tumor volume and mouse body weight were monitored every three days. The tumor volume was determined using the following formula: $V = \alpha\beta^2 / 2$, where "α" represents the longest radius and β the shortest radius of the tumor.

Following blood collection under anesthesia after three treatments, the mice were euthanized by cervical dislocation under 2–3% isoflurane anesthesia. The tumor samples were collected, weighed, and stored at −80 °C or fixed in 10% formalin. The heart, liver, spleen, lungs, and kidneys were excised and fixed in 10% formalin.

Release of RA in Tumors

The RM1 tumor model was established as previously described. When the tumor volume reached 100–150 mm^3, the mice were randomly divided into two groups, RA (4 mg/kg) and LRA (4 mg/kg, on the RA basis), with five mice in each group. The mice were sacrificed 48 h after treatment and the tumors were collected. Double-distilled water (dd-H_2O) was added at a volume of 100 μL per 0.1 g tumor tissue, followed by grinding into tissue homogenates. Mixtures of homogenates with methanol (1:3, v/v) were prepared and centrifuged at 10,000 g for 10 min at 4 °C. Supernatants were collected and passed through a 0.22 μm filter. Finally, RA was quantified by HPLC.

H&E Staining, TUNEL Staining, and Immunohistochemical Staining

Paraffin-embedded tumor samples were cut into 4 μm consecutive sections, and H&E staining,[28] TUNEL staining,[29] and immunohistochemical staining[30] were performed according to the manufacturer's protocols and previous studies.

For H&E staining, after dewaxing and hydration in water, the sections were stained with hematoxylin solution for 10 min and Eosin Y Aqueous solution for 30s, dehydrated, and covered. Images were captured under a light microscope (Olympus, Tokyo, Japan).

For TUNEL staining, the sections were dropwise added with 100 μL 0.1% Triton X-100-PBS solution and incubated at room temperature for 10 min. Thereafter, the sections were labeled with 50 μL TdT working solution at 37 °C for 1 h in the dark. Next, 100 μL 0.1% Triton X-100-PBS solution was added dropwise before mounting with ProLong Glass Antifade Mountant Medium (Invitrogen, Cat#P36980). Images were captured using a fluorescence microscope (Olympus).

For immunohistochemical staining, the sections were deparaffinized and hydrated in water. Epitope retrieval was then performed by heating with EDTA retrieval buffer (Solarbio, Cat#C1033), and nonspecific binding was performed with 2% BSA for 2 h at room temperature. Next, the sections were immunostained with primary antibodies including anti-HMGB1 (1:200), anti-Bcl-2 (1:500), anti-cleaved-Caspase-3 (1:100), anti-Ki67 (1:100), and anti-AR (1:200) at 4 °C

overnight. After that, the sections were incubated with HRP-conjugated secondary antibody and visualized by the DAB Detection Kit (Thermo Scientific, Cat#34002). Images were captured under a light microscope (Olympus, Tokyo, Japan).

Routine Blood Examination and ELISA Assay

Whole blood samples were collected, and the hemoglobin count (HGB), white blood cell count (WBC), and blood platelet count (PLT) were determined using a hematology analyzer (Shinova, Shanghai, China).

Whole blood samples were centrifuged at 1000 × g for 10 min after standing at room temperature for 20 min, and the serum was collected. ELISA kits were used to determine PSA levels, according to the manufacturer's protocol.

Assessments of Liver and Renal Function

The total bilirubin (T-Bil), alanine aminotransferase (ALT), aspartate aminotransferase (AST), blood urea nitrogen (BUN), uric acid (UA), and creatinine (CREA) levels in serum were measured using an automatic biochemical analyzer.

Masson's Trichrome Staining

Masson's trichrome staining was performed according to the manufacturer's instructions. First, the sections were stained with Weigert's iron hematoxylin solution for 10 min after dewaxing and hydration, differentiated in acid alcohol solution for 10s, and then stained with bluing solution for 3 min, ponceau-acid fuchsin solution for 10 min, and aniline blue solution for 2 min. The cytoplasm was stained red, and collagen was stained blue. Images were captured under a light microscope (Olympus, Tokyo, Japan).

Statistical Analysis

Statistical analysis was performed using ANOVA. Statistical significance was set at $P < 0.05$. All analysis procedures and graphs were performed using GraphPad Prism version 8. Data are expressed as the mean ± SD.

Results

Preparation and Characterization of RA Liposome

The LRA liposome (LRA) was prepared as shown in Figure 1A by hydrating the dried lipid films containing HSPC, CHO, and DSPE-PEG_{2k} with deionized water. Lipid films were prepared, and then RA was loaded into liposomes through physical interactions. Free RA was removed by dialysis, and LRA was obtained after filtration and lyophilization. Trehalose was used during lyophilization to protect LRA nanoparticles. The quantity of RA was measured by high-performance liquid chromatography (HPLC), and the drug-loading content of LRA was 4.0%. The diameter of LRA was 173.5 ± 15.3 nm (Figure 1B), as analyzed by DLS. This phenomenon was caused by water, and the liposome diameter was larger in water than in dry conditions because of the amphiphilic characteristics of liposomes.

The stability of LRA was evaluated in phosphate buffered saline (PBS) at pH 7.4 (Figure 1C). The diameter of LRA was measured by DLS at different time points, including 0, 1, 2, 6, and 24 h. The results revealed that LRA was stable in PBS (pH 7.4) for 24 h.

The in vitro release behavior of LRA was studied in phosphate buffered saline (PBS) at different pH (pH 7.4, pH 6.8) at 37 °C. At different time points (0, 1, 4, 24, 48, and 72 h), the released RA was analyzed by HPLC. The results revealed that RA could be released gently at pH 7.4 and pH 6.8 (Figure 1D). The RA release in pH 6.8 buffer was greater than that at pH 7.4, indicating that more RA could be released from LRA in tumors than under physiological conditions, as it has been proven that acidity is a common feature of a tumor.[31]

Effects of RA and LRA on Cell Activity in vitro

Firstly, prostate cancer cell RM1 was treated with 1.5 and 3 μM of LRA/Rh for 0.5, 3, and 5 h to investigate its internalization ability of LRA. It is hard to locate the fluorescent signal in the treatment group of 1.5 μM LRA/Rh in the first 0.5 h. However, the fluorescence intensity was enhanced in a dose- and time-dependent manner (Figure 2A). At 3 h, fluorescence in the 1.5

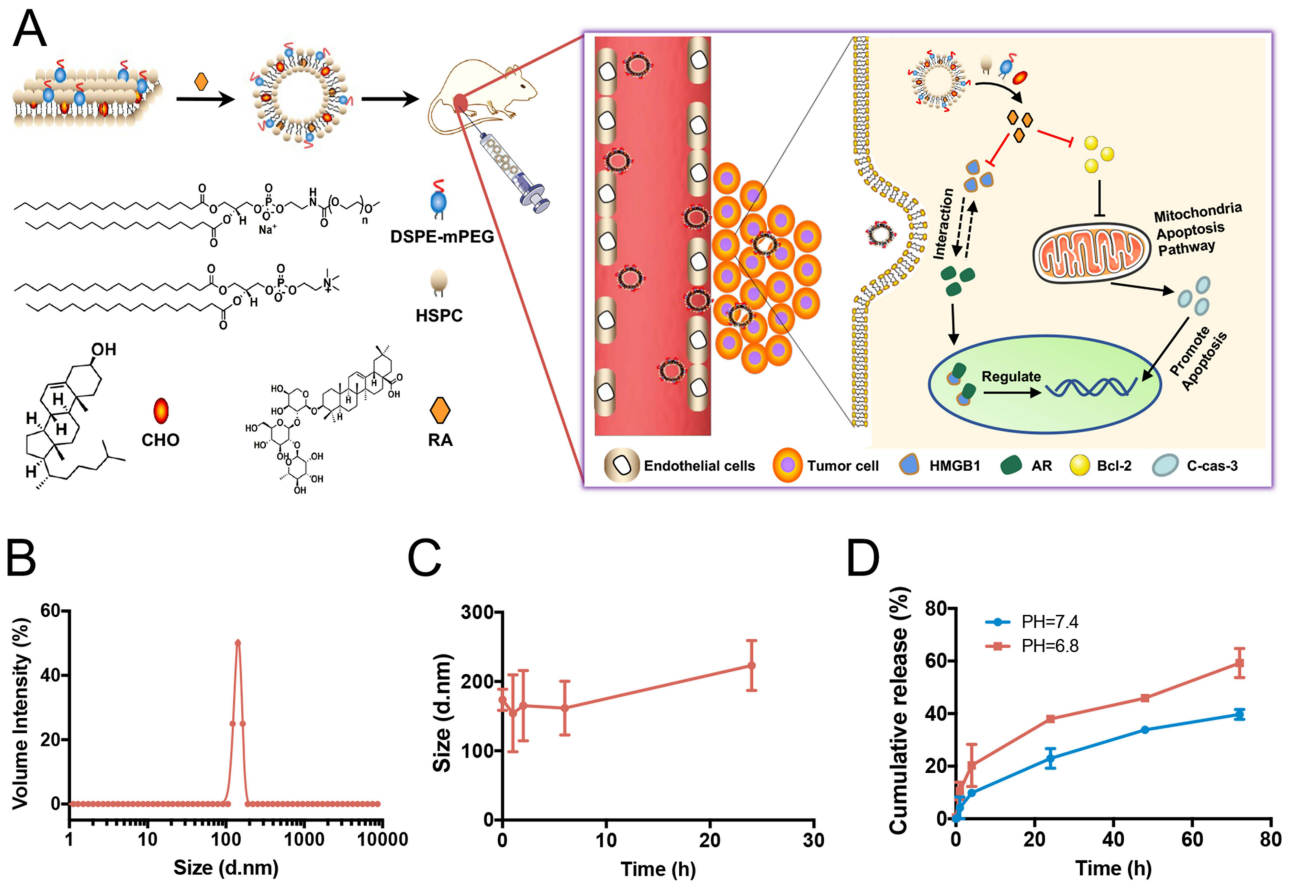

Figure 1 Preparation and characterization of RA liposome. (**A**) Synthesis of LRA. (**B**) The diameter of LRA analyzed by DLS. (**C**) The stability of LRA. (**D**) The in vitro release behavior of LRA.

μM LRA/Rh treatment group was mostly observed at the cellular surface. However, fluorescence could be clearly observed throughout the RM1 cells in the group of 1.5 μM LRA/Rh at 5 h and the group of 3 μM LRA/Rh at 3 and 5 h.

The cytotoxic effects of RA and LRA on the two prostate cancer cell lines RM1 and 22Rv1 were determined using an MTT assay. The cells were exposed to different concentrations of RA and LRA, ranging from 0 to 12 μM, for 24, 48, and 72 h. The cellular toxicity of RA and LRA was enhanced in a time- and dose-dependent manner. For RM1 cells (Figure 2B), 1.5 μM RA could induce an almost 50% inhibitory rate at 48 h, and the inhibitory rate continued to rise with increased concentration and time, finally reaching 100% inhibition when treated with 12 μM RA for 72 h. This inhibitory trend was also observed in the LRA treatment groups. At the same dose, LRA required a longer treatment duration to achieve the same inhibition rate as RA. A dose-dependent cellular inhibitory capacity was also observed in 22Rv1 cells after treatment with RA or LRA (Figure 2C). However, at the same dose, the inhibitory effect of RA and LRA on 22Rv1 cells was not as effective as that on RM1 cells. A 50% cell inhibition rate required 6 μM RA treatment for 72 h.

To verify the effects of RA and LRA on the proliferation of prostate cancer cells, a colony formation assay was performed. Cell clonality was significantly decreased after treatment with RA and LRA in a dose-dependent manner in both prostate cancer cell lines (Figure 2D).

Western blot showed that the expressions of AR and HMGB1 were significantly downregulated after treatment with RA or LRA in these two prostate cancer cell lines. Similar to the MTT results, at the same drug concentration, downregulation of the RM1 protein content was more significant than that of 22Rv1 (Figure 2E and F).

Effects of RA and LRA on Cell Apoptosis in vitro

To gain insight into the mechanism by which RA and LRA affect the viability of RM1 and 22Rv1 cells, the cell cycle and apoptosis were detected by PI and Annexin V-PI staining, respectively. As shown in Figure 3A and B, there was no

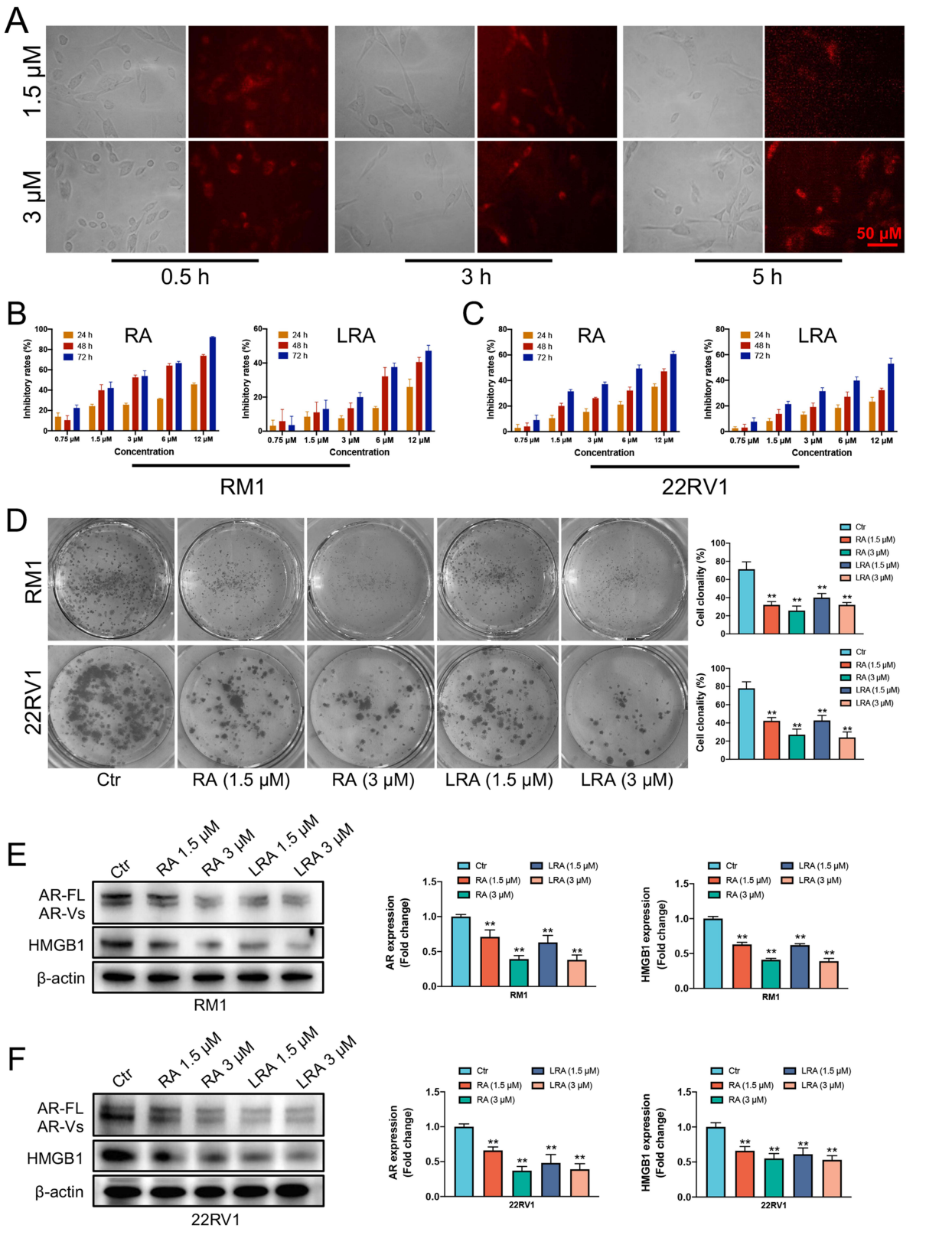

Figure 2 Effects of RA and LRA on cell activity in vitro. (**A**) The internalization ability of LRA. (**B** and **C**) Inhibitory effects of different doses of RA and LRA on RM1 and 22Rv1 cells. (**D**) Cell clonality of RM1 and 22Rv1 cells. (**E** and **F**) Expression of AR and HMGB1 detected by Western blot and semi-quantification of the Western blot analysis on RM1 and 22Rv1 cells. Data are expressed as the mean ± SD, n = 3. **P<0.01 vs Ctrl.

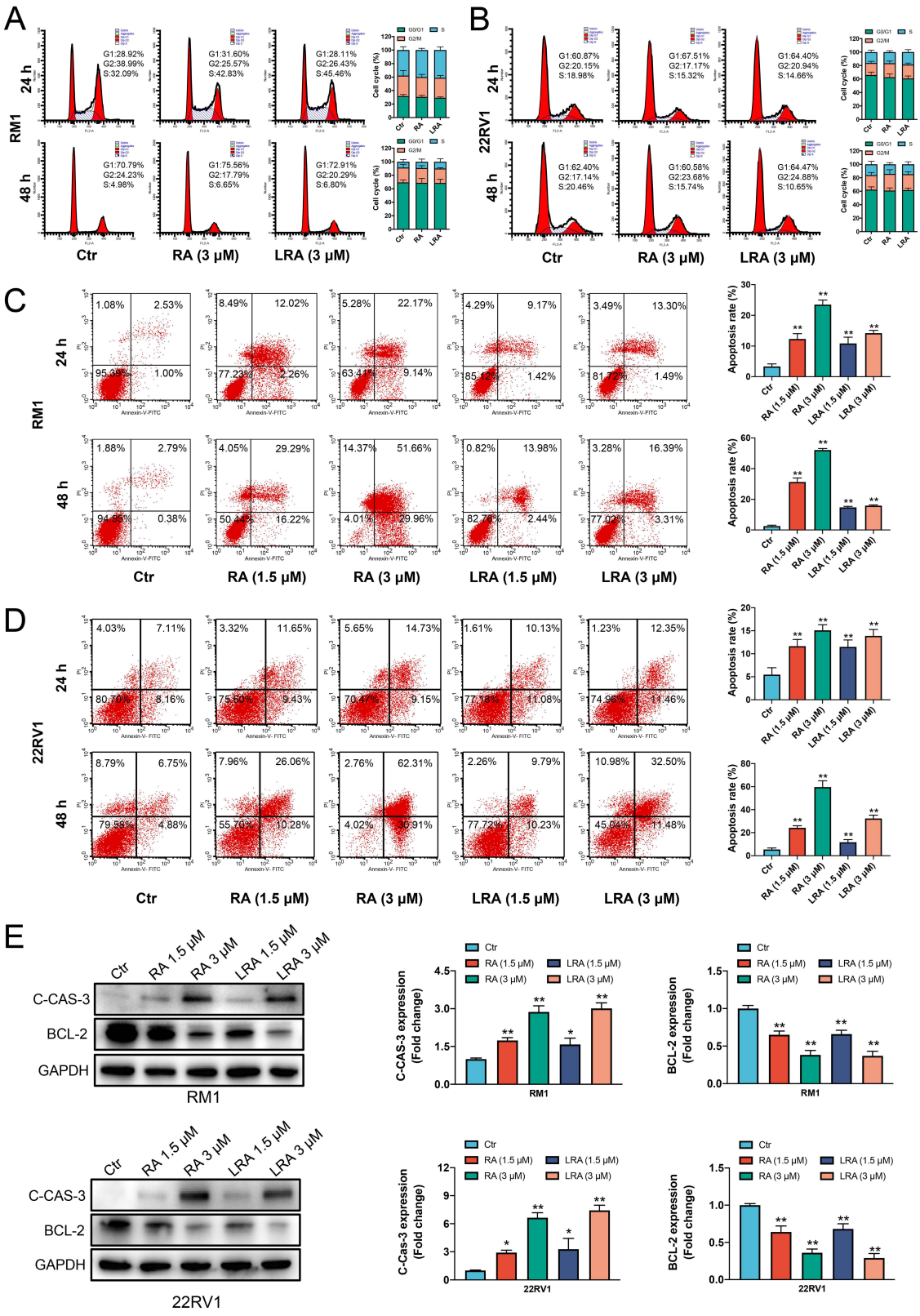

Figure 3 Promotion of cellular apoptosis by RA and LRA. (**A** and **B**) Flow cytometric and statistical analysis of cell cycle proportions of RM1 and 22Rv1. (**C** and **D**) Flow cytometric and statistical analysis of cell apoptosis of RM1 and 22Rv1. (**E**) Expression of cleaved-Caspase-3 and Bcl-2 detected by Western blot and semi-quantification of the Western blot analysis. Data are expressed as the mean ± SD, n = 3. *P<0.05, **P<0.01 vs Ctrl.

change in the cell cycle of either cell line at different doses or intervention durations. In contrast, the apoptotic rate of RA and LRA was significantly higher than that in the control group in both RM1 (Figure 3C) and 22Rv1 (Figure 3D) cells. To further investigate the mechanism underlying the effects of RA and LRA on this process, apoptosis-related proteins were measured using Western blot (Figure 3E). The expression of Bcl-2, a major apoptosis suppressing protein,[32] was downregulated in the RA and LRA treatment groups. Moreover, the protein level of cleaved-Caspase-3, a reliable mediator of apoptosis activation,[33] in the RA and LRA groups was significantly higher than that in the control group. These results indicate that apoptosis participates in RA-induced or LRA-induced cell death in prostate cancer cells.

Antitumor Efficacy of RA and LRA in vivo

The distribution of free RA in tumors was tested to investigate the active drug release of LRA in tumors. Nanoparticles have been widely studied for their ability to passively target tumors because of their enhanced permeability and retention effect (EPR) effect.[34] At 48 h post injection, the concentration of free RA in the LRA group was significantly higher than that in the RA group (Figure 4A).

To further clarify the therapeutic effects of RA and LRA on PCa, a prostate cancer model was constructed using C57BL/6 mice with RM1 cells. After treatment with RA or LRA, the results showed an evident inhibition of both tumor volume and tumor weight in the RA and LRA groups compared with the control group, while LRA treatment showed a better therapeutic effect than RA treatment (Figure 4B–D). In addition, the serum level of PSA, an AR-regulated gene, decreased in the RA and LRA groups compared to that in the control group, with the same tendency as the decrease in tumor growth (Figure 4E). The number of nuclei with fragmentation and pyknosis was higher in the LRA group than in the RA group (Figure 4F).

To further verify that RA and LRA induced apoptosis, TUNEL staining was performed. As shown in Figure 4G, the green fluorescence signal which represents apoptotic cells indicated that RA and LRA markedly induced tumor apoptosis compared with the control group.

Immunohistochemical staining was performed to evaluate the expression of the cell proliferation marker Ki67 (Figure 4H), the prostate cancer-related signaling pathway HMGB1 and AR (Figure 4I), and the apoptosis markers cleaved-Caspase-3 and Bcl-2 (Figure 4J). The highest levels of Ki67, HMGB1, AR, and Bcl-2 were observed in the control group, whereas they were downregulated in the RA and LRA groups. The expression of cleaved-Caspase-3 was increased after treatment with RA and LRA compared with that in the control group. Furthermore, the results of Western blot were consistent with those of IHC staining (Figure 4K and L). These results suggest that RA and LRA inhibit prostate cancer development by inducing apoptosis in vivo.

Biosafety Assessments of RA and LRA

The results of our previous experiments indicate that intraperitoneal injection of RA could induce serious adverse effects in mice. Thus, biosafety assessments were conducted to verify whether LRA could avoid the same adverse effects as RA. As shown in Figure 5A, RA treatment significantly decreased the body weight of mice, whereas LRA treatment did not exhibit the same side effects. The results of routine blood examinations showed no significant differences in terms of HGB (Figure 5B), WBC (Figure 5C), or PLT (Figure 5D) in each group. Biochemical parameters, including liver function indices T-Bil, ALT, and AST, and kidney function indices BUN, UA, and CREA, were also measured. The results showed that RA treatment upregulated the levels of T-Bil, ALT, and AST, whereas LRA alleviated these impairments (Figure 5E–G). No significant differences were found in BUN, UA, or CREA levels between the groups (Figure 5H–J).

H&E staining results showed no significant changes in the heart, spleen, lung, and kidney among the three groups. However, necrotic and vacuous areas in the liver were observed in the RA group but not in the LRA group (Figure 5K). Masson's staining was performed to evaluate the degree of liver fibrosis in each group (Figure 5L). Collagen (blue staining) was obviously increased in the RA group compared to the control and LRA groups. These results demonstrate that LRA effectively alleviated the side effects of RA.

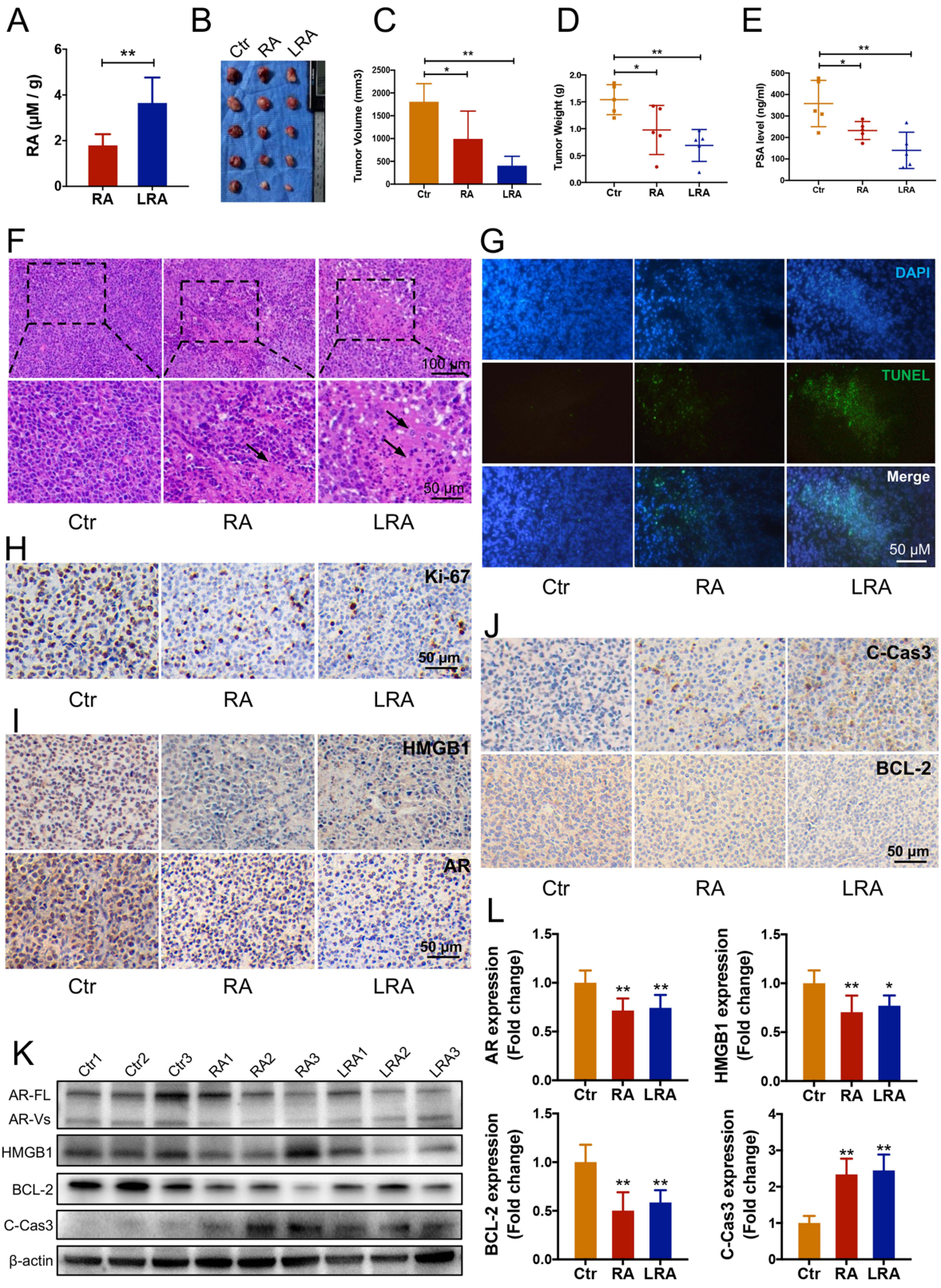

Figure 4 Antitumor efficacy of RA and LRA in vivo. (**A**) Free RA distribution in the tumor. (**B**–**D**) Visual representation of tumors and their volume and weight. (**E**) The level of PSA in serum. (**F**) The H&E staining of tumors. (**G**) The TUNEL staining of tumors. (**H**–**J**) The immunohistochemical staining of Ki-67, HMGB1, AR, cleaved-Caspase -3, and Bcl-2 in tumors. (**K**–**L**) Expression of HMGB1, AR, cleaved-Caspase-3, and Bcl-2 detected by Western blot and semi-quantification of the Western blot analysis. Data are expressed as the mean ± SD, n = 5. *P<0.05, **P<0.01 vs Ctrl.

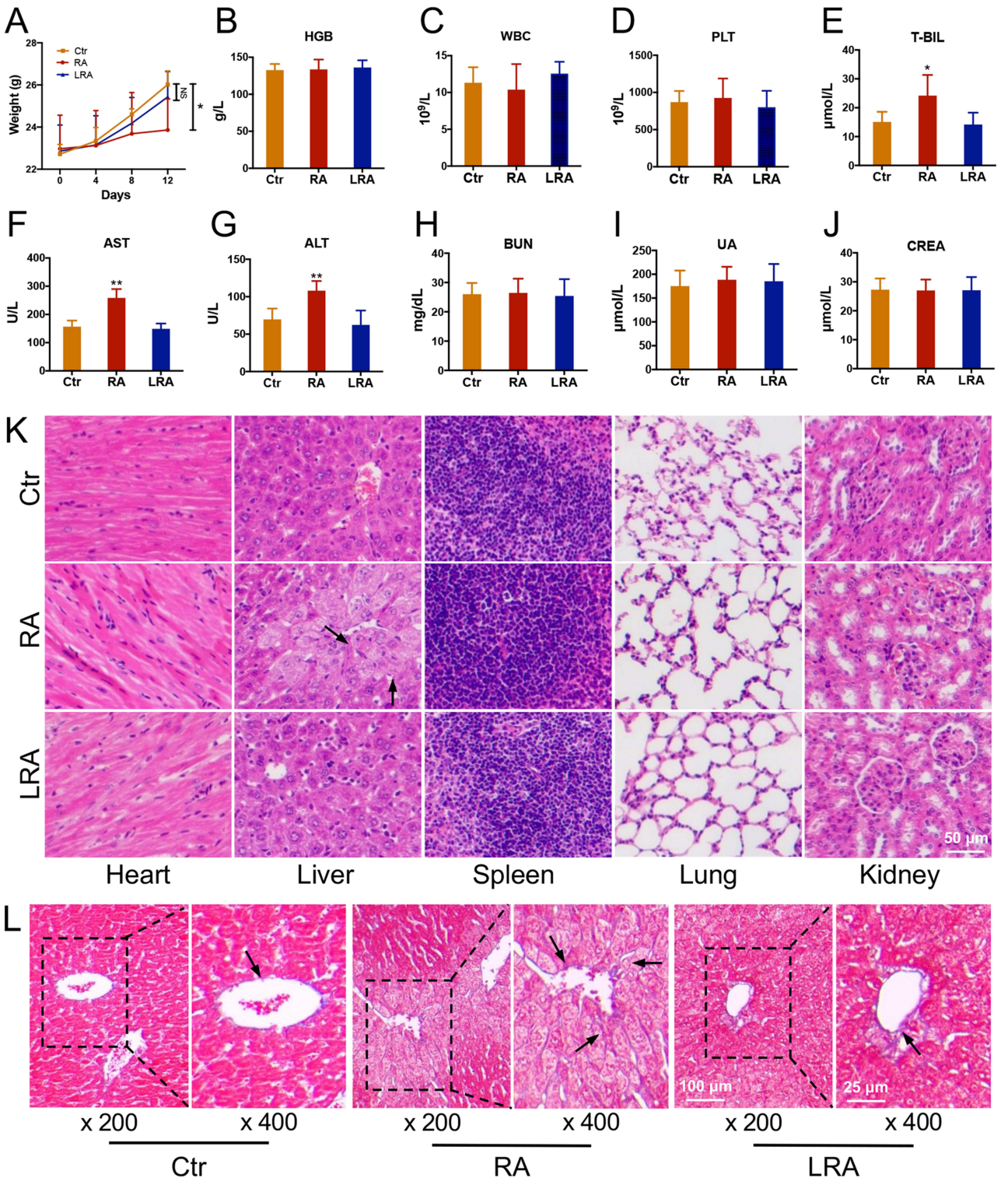

Figure 5 Biosafety assessments of RA and LRA. (**A**) The body weight changes in each group. (**B**–**D**) The routine blood examinations of HGB, WBC, and PLT. (**E**–**J**) The biochemical parameter analysis of liver function indexes T-Bil, ALT, and AST, and kidney function indexes BUN, UA, and CREA. (**K**) The H&E staining of the histological changes of the heart, liver, spleen, lung, and kidney. (**L**) The Masson staining of the liver. Data are expressed as the mean ± SD, n = 5. *P<0.05, **P<0.01 vs Ctrl.

Discussion

In this study, RA-loaded liposome (LRA), a classical drug delivery system, was developed using HSPC, DSPE-PEG_{2K}, CHO, and RA. Moreover, LRA enhanced the therapeutic effect, reduced side effects, and improved bioavailability compared to RA in prostate cancer both in vivo and in vitro.

The antitumor ability of RA has been demonstrated in various cancer types, such as suppressing proliferation and induction of apoptosis in non-small cell lung cancer by suspending the expression of STAT3,[35] inducing apoptosis in osteosarcoma by modulating the signaling pathways of JNK/c-Jun,[36] and inducing apoptosis in colorectal cancer by decreasing the activity of the Wnt/β-catenin signaling pathway.[37] The proliferation inhibitory effect of RA on prostate cancer cells, associated with its targeted inhibition of AR, has been proven in vitro,[13] whereas the inhibitory effect of RA on prostate cancer in vivo was first evaluated in this study. However, hepatotoxicity, weight loss, and other biological side effects have also been observed following RA treatment. Therefore, a drug delivery system is required to target the delivery of drugs to the tumor site to ensure that the drug is effective while reducing adverse effects.

We applied liposome to contribute to this delivery system, as it has been proven that the drug loaded inside the liposome could minimize its side effects compared to the free drug alone.[38] Studies have reported that estrogen-targeted oxaliplatin liposomes could improve the toxicity of oxaliplatin in gastric cancer[39] and doxorubicin (DOX) liposomes loaded with Schizandrin A could improve the bioavailability and reduce the side effects of DOX alone in the treatment of liver cancer.[40]

In the classical LRA drug delivery system constructed in this study, HSPC served as the basic framework of liposomes and CHO was added to enhanced its stability.[41] Simultaneously, DSPE-PEG_{2k} was added to increase its circulation lifetime.[42] The longer circulation lifetime was related to the longer chain of PEG, as the blood concentration of PEG_{1900}-liposome was higher than that of PEG_{750}-liposome.[43] The enhanced permeation and retention (EPR) effect is a remarkable characteristic of tumor tissue that can assemble more nanocarriers in malignant tissue by penetrating incomplete tumor vessels, and is also known as the passive targeting of nanoparticles.[44] The results of in vivo experiments in this study revealed a better antitumor effect of LRA than that of RA.

To further explore the mechanism underlying the therapeutic effect of RA and LRA on prostate cancer, cell cycle and apoptosis were analyzed. In addition, the apoptosis-related proteins Bcl-2 and cleaved-Caspase-3 were evaluated. These results indicated that both RA and LRA induced cell apoptosis, which is in accordance with previous studies.[13] Chen et al determined that HMGB1 and AR are strongly associated with the development of CRPC, at least partly because HMGB1 interacts with AR and reactivates the AR signaling pathway, suggesting that targeting HMGB1 might be a novel strategy for CRPC therapy.[8] The results of this study showed that both RA and LRA could downregulate the expression of HMGB1 and silence the AR signaling pathway. Furthermore, the AR signaling pathway is involved in the regulation of a series of intracellular processes, including cell proliferation and apoptosis.[45] Thus, we suspect that the mechanism by which RA and LRA induce apoptosis in prostate cancer cells may be related to the AR signaling pathway, and subsequent studies should further investigate the underlying mechanism.

The most inspiring results of this study are that LRA not only enhanced the antitumor effect compared to RA, but also reduced the side effects of RA. Protection from body weight loss is the most intuitive manifestation of the low toxicity of LRA. Masson staining and measurement of liver function indicators indicated that LRA was less hepatotoxic than RA.

Conclusion

LRA was prepared by a thin-film hydration method using HSPC, DSPE-PEG_{2K}, CHO, and RA. This nanosized LRA drug delivery system exhibited a stable structure and sustained drug release. Moreover, RA and LRA significantly inhibited the growth of prostate cancer cells by promoting cell apoptosis, both in vivo and in vitro. Furthermore, LRA resulted in less body weight loss and hepatotoxicity than RA alone. These results suggest that RA-loaded liposome could be a drug delivery system for prostate cancer therapy in further clinical applications.

Abbreviations

RA, Raddeanin A; HSPC, hydrogenated soybean phospholipids; DSPE-PEG2k, 1.2-distearoyl-sn-glycero-3-phosphoethanolamine-N-Polyethyleneglycol-2000 (sodium salt); CHO, cholesterol; LRA, RA-loaded liposome; PCa, prostate cancer; HMGB1, high-mobility Group Protein B1; AR, androgen receptors; ADT, androgen deprivation therapies; CRPC, castration-resistant prostate cancer; HPLC, high performance liquid chromatography; T-Bil, total bilirubin, ALT, alanine aminotransferase; AST, aspartate aminotransferase; BUN, blood urea nitrogen; UA, uric acid; CREA, creatinine; EGCG, epigallocatechin-3-gallate; HA, polyethylene glycol gelatin hyaluronic acid.

Data Sharing Statement

The datasets used and/or analyzed during the current study are available from the corresponding author upon reasonable request.

Ethics Approval and Consent to Participate

All animal experiments were approved by the Experimental Animal Ethics Committee of Jilin University (Changchun, China).

Author Contributions

All authors made a significant contribution to the work reported, whether that is in the conception, study design, execution, acquisition of data, analysis and interpretation, or in all these areas; took part in drafting, revising or critically reviewing the article; gave final approval of the version to be published; have agreed on the journal to which the article has been submitted; and agree to be accountable for all aspects of the work.

Funding

This work was supported by grants from the Jilin Provincial Department of Science and Technology Project (grant number:20210204200YY) and the National Natural Science Foundation of China (52003100).

Disclosure

The authors declare that they have no competing interests in this work.

References

1. Miller KD, Nogueira L, Devasia T, et al. Cancer treatment and survivorship statistics, 2022. *CA Cancer J Clin*. 2022;72:409–436. doi:10.3322/caac.21731
2. Rebello RJ, Oing C, Knudsen KE, et al. Prostate cancer. *Nat Rev Dis Primers*. 2021;7(1):9. doi:10.1038/s41572-020-00243-0
3. Teo MY, Rathkopf DE, Kantoff P. Treatment of advanced prostate cancer. *Annu Rev Med*. 2019;70:479–499. doi:10.1146/annurev-med-051517-011947
4. Khan A, Mao Y, Tahreem S, Wei DQ, Wang Y. Structural and molecular insights into the mechanism of resistance to enzalutamide by the clinical mutants in androgen receptor (AR) in castration-resistant prostate cancer (CRPC) patients. *Int J Biol Macromol*. 2022;218:856–865. doi:10.1016/j.ijbiomac.2022.07.058
5. Jamroze A, Chatta G, Tang DG. Androgen receptor (AR) heterogeneity in prostate cancer and therapy resistance. *Cancer Lett*. 2021;518:1–9. doi:10.1016/j.canlet.2021.06.006
6. Shafi AA, Yen AE, Weigel NL. Androgen receptors in hormone-dependent and castration-resistant prostate cancer. *Pharmacol Ther*. 2013;140(3):223–238. doi:10.1016/j.pharmthera.2013.07.003
7. Xue J, Suarez JS, Minaai M, et al. HMGB1 as a therapeutic target in disease. *J Cell Physiol*. 2021;236(5):3406–3419. doi:10.1002/jcp.30125
8. Chen J, Xu D, Wang T, et al. HMGB1 promotes the development of castration-resistant prostate cancer by regulating androgen receptor activation. *Oncol Rep*. 2022;48(5). doi:10.3892/or.2022.8412
9. Guan YY, Liu HJ, Luan X, et al. Raddeanin A, a triterpenoid saponin isolated from Anemone raddeana, suppresses the angiogenesis and growth of human colorectal tumor by inhibiting VEGFR2 signaling. *Phytomedicine*. 2015;22(1):103–110. doi:10.1016/j.phymed.2014.11.008
10. Li JN, Yu Y, Zhang YF, Li ZM, Cai GZ, Gong JY. Synergy of Raddeanin A and cisplatin induced therapeutic effect enhancement in human hepatocellular carcinoma. *Biochem Biophys Res Commun*. 2017;485(2):335–341. doi:10.1016/j.bbrc.2017.02.079
11. Peng Z, Zhang C, Zhou W, Wu C, Zhang Y. The STAT3/NFIL3 signaling axis-mediated chemotherapy resistance is reversed by Raddeanin A via inducing apoptosis in choriocarcinoma cells. *J Cell Physiol*. 2018;233(7):5370–5382. doi:10.1002/jcp.26362
12. Shen X, Li L, He Y, Lv X, Ma J. Raddeanin A inhibits proliferation, invasion, migration and promotes apoptosis of cervical cancer cells via regulating miR-224-3p/Slit2/Robo1 signaling pathway. *Aging*. 2021;13(5):7166–7179. doi:10.18632/aging.202574
13. Xia H, Hu C, Bai S, et al. Raddeanin A down-regulates androgen receptor and its splice variants in prostate cancer. *J Cell Mol Med*. 2019;23(5):3656–3664. doi:10.1111/jcmm.14267
14. Gu G, Qi H, Jiang T, et al. Investigation of the cytotoxicity, apoptosis and pharmacokinetics of Raddeanin A. *Oncol Lett*. 2017;13(3):1365–1369. doi:10.3892/ol.2017.5588
15. Liu Y, Ma B, Zhang Q, et al. Development and validation of a sensitive liquid chromatography/tandem mass spectrometry method for the determination of raddeanin A in rat plasma and its application to a pharmacokinetic study. *J Chromatogr B Analyt Technol Biomed Life Sci*. 2013;912:16–23. doi:10.1016/j.jchromb.2012.09.038
16. Bangham AD, Horne RW. Negative staining of phospholipids and their structural modification by surface-active agents as observed in the electron microscope. *J Mol Biol*. 1964;8:660–668. doi:10.1016/s0022-2836(64)80115-7
17. Zahednezhad F, Saadat M, Valizadeh H, Zakeri-Milani P, Baradaran B. Liposome and immune system interplay: challenges and potentials. *J Control Release*. 2019;305:194–209. doi:10.1016/j.jconrel.2019.05.030
18. Vedovatto S, Facchini JC, Batista RK, Paim TC, Lionzo MIZ, Wink MR. Development of chitosan, gelatin and liposome film and analysis of its biocompatibility in vitro. *Int J Biol Macromol*. 2020;160:750–757. doi:10.1016/j.ijbiomac.2020.05.229

19. Yaroslavov AA, Efimova AA, Krasnikov EA, et al. Chitosan-based multi-liposomal complexes: synthesis, biodegradability and cytotoxicity. *Int J Biol Macromol*. 2021;177:455–462. doi:10.1016/j.ijbiomac.2021.02.169
20. Gao W, Li L, Zhang X, et al. Nanomagnetic liposome-encapsulated parthenolide and indocyanine green for targeting and chemo-photothermal antitumor therapy. *Nanomedicine*. 2020;15(9):871–890. doi:10.2217/nnm-2019-0038
21. Vazquez Fuster IB, Taylor AR, Smith AN, et al. Pharmacokinetics of multivesicular liposomal encapsulated cytarabine when administered subcutaneously in dogs. *J Vet Intern Med*. 2020;34(4):1563–1569. doi:10.1111/jvim.15809
22. Jeon M, Kim G, Lee W, Baek S, Jung HN, Im HJ. Development of theranostic dual-layered Au-liposome for effective tumor targeting and photothermal therapy. *J Nanobiotechnology*. 2021;19(1):262. doi:10.1186/s12951-021-01010-3
23. Akanda MH, Rai R, Slipper IJ, et al. Delivery of retinoic acid to LNCap human prostate cancer cells using solid lipid nanoparticles. *Int J Pharm*. 2015;493(1–2):161–171. doi:10.1016/j.ijpharm.2015.07.042
24. Lee JB, Zhang K, Tam YYC, et al. A Glu-urea-Lys ligand-conjugated lipid nanoparticle/siRNA system inhibits androgen receptor expression in vivo. *Mol Ther Nucleic Acids*. 2016;5(8):e348. doi:10.1038/mtna.2016.43
25. Saralkar P, Dash AK. Alginate nanoparticles containing curcumin and resveratrol: preparation, characterization, and in vitro evaluation against DU145 prostate cancer cell line. *AAPS PharmSciTech*. 2017;18(7):2814–2823. doi:10.1208/s12249-017-0772-7
26. Kapoor M, Lee SL, Tyner KM. Liposomal drug product development and quality: current US experience and perspective. *Aaps J*. 2017;19(3):632–641. doi:10.1208/s12248-017-0049-9
27. Chen J, Xia Y, Peng Y, et al. Analysis of the association between KIN17 expression and the clinical features/prognosis of epithelial ovarian cancer, and the effects of KIN17 in SKOV3 cells. *Oncol Lett*. 2021;21(6):475. doi:10.3892/ol.2021.12736
28. Wu S, Zhao F, Zhao J, et al. Dioscin improves postmenopausal osteoporosis through inducing bone formation and inhibiting apoptosis in ovariectomized rats. *Biosci Trends*. 2019;13(5):394–401. doi:10.5582/bst.2019.01186
29. Ge J, Liu J, Wang T, et al. Prolonged exposure to the herbicide atrazine suppresses immune cell functions by inducing spleen cell apoptosis in rats. *Ecotoxicol Environ Saf*. 2021;220:112386. doi:10.1016/j.ecoenv.2021.112386
30. Kong D, Chen J, Sun X, et al. GRIM-19 over-expression represses the proliferation and invasion of orthotopically implanted hepatocarcinoma tumors associated with downregulation of Stat3 signaling. *Biosci Trends*. 2019;13(4):342–350. doi:10.5582/bst.2019.01185
31. Boedtkjer E, Pedersen SF. The acidic tumor microenvironment as a driver of cancer. *Annu Rev Physiol*. 2020;82:103–126. doi:10.1146/annurev-physiol-021119-034627
32. Khawaja H, Briggs R, Latimer CH, et al. Bcl-xL is a key mediator of apoptosis following KRASG12C inhibition in KRASG12C mutant colorectal cancer. *Mol Cancer Ther*. 2022. doi:10.1158/1535-7163.Mct-22-0301
33. Shalini S, Dorstyn L, Dawar S, Kumar S. Old, new and emerging functions of caspases. *Cell Death Differ*. 2015;22(4):526–539. doi:10.1038/cdd.2014.216
34. Pérez-Herrero E, Fernández-Medarde A. Advanced targeted therapies in cancer: drug nanocarriers, the future of chemotherapy. *Eur J Pharm Biopharm*. 2015;93:52–79. doi:10.1016/j.ejpb.2015.03.018
35. Li L, Chen M, Li G, Cai R. Raddeanin A induced apoptosis of non-small cell lung cancer cells by promoting ROS-mediated STAT3 inactivation. *Tissue Cell*. 2021;71:101577. doi:10.1016/j.tice.2021.101577
36. Wang Z, Shen J, Sun W, et al. Antitumor activity of Raddeanin A is mediated by Jun amino-terminal kinase activation and signal transducer and activator of transcription 3 inhibition in human osteosarcoma. *Cancer Sci*. 2019;110(5):1746–1759. doi:10.1111/cas.14008
37. Wang Y, Bao X, Zhao A, et al. Raddeanin A inhibits growth and induces apoptosis in human colorectal cancer through downregulating the Wnt/β-catenin and NF-κB signaling pathway. *Life Sci*. 2018;207:532–549. doi:10.1016/j.lfs.2018.06.035
38. Sercombe L, Veerati T, Moheimani F, Wu SY, Sood AK, Hua S. Advances and challenges of liposome assisted drug delivery. *Front Pharmacol*. 2015;6:286. doi:10.3389/fphar.2015.00286
39. Sun Y, Xie Y, Tang H, et al. In vitro and in vivo evaluation of a novel estrogen-targeted PEGylated oxaliplatin liposome for gastric cancer. *Int J Nanomedicine*. 2021;16:8279–8303. doi:10.2147/ijn.S340180
40. Fan Y, Marioli M, Zhang K. Analytical characterization of liposomes and other lipid nanoparticles for drug delivery. *J Pharm Biomed Anal*. 2021;192:113642. doi:10.1016/j.jpba.2020.113642
41. Bozzuto G, Molinari A. Liposomes as nanomedical devices. *Int J Nanomedicine*. 2015;10:975–999. doi:10.2147/ijn.S68861
42. Tan X, Zhu X, Xu D, et al. A mitochondria-targeted nano-platform for pancreatic cancer therapy. *Front Chem*. 2022;10:951434. doi:10.3389/fchem.2022.951434
43. Allen TM, Hansen C, Martin F, Redemann C, Yau-Young A. Liposomes containing synthetic lipid derivatives of poly(ethylene glycol) show prolonged circulation half-lives in vivo. *Biochim Biophys Acta*. 1991;1066(1):29–36. doi:10.1016/0005-2736(91)90246-5
44. Torchilin V. Tumor delivery of macromolecular drugs based on the EPR effect. *Adv Drug Deliv Rev*. 2011;63(3):131–135. doi:10.1016/j.addr.2010.03.011
45. Gan X, Huang H, Wen J, et al. α-Terthienyl induces prostate cancer cell death through inhibiting androgen receptor expression. *Biomed Pharmacother*. 2022;152:113266. doi:10.1016/j.biopha.2022.113266